Military Technical College
Kobry El-Kobbah,
Cairo, Egypt.

18th International Conference on Applied Mechanics and Mechanical Engineering.

NUMERICAL INVESTIGATION OF THE EFFECT OF DIELECTRIC BARRIER DISCHARGE ACTUATOR (DBDA) ON FILM COOLING PERFORMANCE DOWNSTREAM A CIRCULAR HOLE SCHEME OVER A GAS TURBINE VANE PRESSURE SIDE

M. Abdelhares[*,1], O. Hassan[*], M. F. El-Dosoky[*] and M. M. Abdelghany[*]

ABSTRACT

This paper presents a numerical investigation of the effect of DBDA length on film cooling performance downstream a circular hole scheme over a gas turbine vane pressure side. The investigated scheme is that of a set of two DBDAs installed downstream a cooling jet injection hole to damp the effect of the Counter Rotating Vortex Pair (CRVP) accompanying the injected cooling jet. The simulation has been carried out assuming one row of circular holes of a diameter D spaced at 4.5 D in the cross-stream direction and inclined at 22° with the vane pressure side surface. The actuators are located at 0.5 D downstream the injection hole and spaced at a distance = 0.25 D. Five cases of different electrode's length ranging from 1.5 D to 12 D have been investigated under different applied voltages in the range from 10 kV to 60 kV. In all those cases both the blowing and density ratios are assumed constant at values equal 1 and 2, respectively. Then, the effect of changing the blowing ratio on the performance has been studied for the case which exhibit optimum performance where maximum surface effectiveness is achieved for specific actuator length and applied voltage. The obtained results show that, for each considered actuator length, the surface average effectiveness was enhanced with the increase of the applied voltage to a certain limit where a maximum value was obtained, and then the effectiveness decreased with the increase of the voltage. The results indicate that this limit varies with the actuator length in such a way that, the longer the actuator the lower the voltage at which maximum surface average effectiveness occurs.

KEYWORDS

Film cooling, Turbine vane, CRVP and Dielectric barrier discharge

---

[*] Mechanical Power Engineering Department, Faculty of Engineering, Assiut University, Assiut 71516, Egypt.
[1] Corresponding Author, e-mail mohamedhares2011@gmail.com.

Nomenclature

F	force	Cx	axial chord
V	volt	y+	wall distance
ρ	density		
E	electric field	**Subscripts and Superscripts**	
Φ	total electric potential	b	body
ϕ	potential due to external field	r	relative
φ	potential due to the net charge density	*	non-dimensional parameter
D	electric induction	m	mainstream
ε	permittivity	i	injected coolant
λ_d	Debye length	c	charge, centerline or coolant
u	velocity component in the x-direction	s	spatially
U	average velocity	**Abbreviations**	
τ	stress tensor	adw	adiabatic wall
ω	vorticity	AC	alternative current
η	cooling effectiveness	BR	blowing ratio
T	temperature	DR	density ratio
α	injection angle	CRVP	counter rotating vortex pair
K_H	heat conduction coefficient	DBDA	dielectric barrier discharge actuator
ϵ	thermodynamic internal energy	EHD	electrohydrodynamic

INTRODUCTION

In film cooling a coolant jet is injected in the boundary layer over metal surfaces to isolate it from surrounded hot stream. In highly temperature working environment, particularly inside gas turbines, film cooling is very significant and highly recommended to be used to extend the expected operating life of the turbine blades. Therefore, for several past years, film cooling has been highly used in gas turbine engines more than any other cooling technique as reported by Goldstein [1]. In such

engines, film cooling is achieved through the use of discrete cylindrical holes as reported by Bunker [2] to deliver injected cold stream from a plenum onto the turbine blades surface to make a thermal insulation between the hot main stream and those surfaces. However, the interaction between the cold jet and the hot main stream generates a Counter Rotating Vortex Pair (CRVP) as demonstrated by Li et al.[3], and Sinha et al. [4]. This vortex pushes the injected coolant jet out and detaches it from the surface. Consequently, it reduces the film cooling effectiveness. Numerous studies have been conducted during the last few years with main objectives to weaken the harmful effects of CRVP on film cooling performance and effectiveness. As described in the literature, this can be accomplished by using either shaped holes or an auxiliary anti-vortex generator to counteract the effect of CRVP.

In the first method, using shaped holes the coolant is initially injected through a round entry whose shape is then expanded or changed at the exit region to provide lower momentum and achieve wider spreading over the metal surface as presented by Bunker [2]. Shaped holes have numerous different geometries that include fan-shaped, laidback, conical and trenches. In the second method, an auxiliary vortex generator generates vortex that acts as anti-CRVP and damps its effect. Generating vortex technique is primarily a flow control technique whose effect in mitigating the CRVP action depends on the generated vortex location and strength. In this technique, the common anti-vortex generators include the use of chevron as shown by Abdala and Elwekeel [5], one-inlet double-outlet hole as presented by Li and Zhang [6], backward injection holes as presented by Park et al. [7], or ramp upstream of the injection holes as presented by Na and Shih.[8] and Zhou and Hu. [9], etc.

Dielectric Barrier Discharge Actuator (DBDA) which has been used for the last decade as an active flow controller consists of an exposed electrode and encapsulated electrode insulated with a dielectric material and a AC power source connected to the two electrodes as presented by Bouchmal [10] and shown in Fig. 1. When a suitable AC voltage is applied to the electrodes the air located in the area of electrodes is ionized and an electric discharge is generated above the encapsulated electrode. The accelerated ionized air from the anode to the cathode in the presence of the electric field produced near the electrodes induces an electrohydrodynamic (EHD) force. This induced force act as an external body force that directly affect the momentum of the mainstream boundary layer. This effect can be employed in controlling the boundary layer and delay its separation. Compared to other flow controlling techniques, the DBDA has several advantages that include low power consumption, no moving parts, low weight and flexibility of use.

During the last couple of years, a vast and special attention has been directed from researchers and scientists toward DBDA actuators technology development as well as towards improving its performance and enhancing its cooling effectiveness. Wang and Roy[11] investigated the effect of geometrical changes of DBDA located at the hole exit for improving film cooling performance. Yu et al.[12] studied the film cooling performance with DBDA and reported that position, power input, and the numbers of DBDAs used have significant effects on film cooling effectiveness. Dai et al. [13] used a pair of DBDAs to produce anti- vortex pair opposite to CRVP and investigated the influence of different geometrical parameters on the performance at different blowing ratios. They found that the optimum DBDA geometrical parameters are directly related to the CRVP strength. Dai et al. [14] investigated the effect of using

DBDA with different hole-shaped schemes. They reported that the fan-shaped hole exhibits an optimum surface attachment and gives the lowest CRVP strength.

In present study, the effect of varying DBDA length and applied voltage on film cooling performance downstream a circular hole scheme has been numerically investigated. The studied scheme is that of a plasma actuator using a pair of DBDAs installed downstream the cooling jet of an injection hole on the pressure side of a turbine vane. The objective of the present paper is a part of a comprehensive study objective to determine the optimum geometrical parameters of the DBDA as well as the optimum operating parameters that lead to best enhancement of the cooling effectiveness of the considered scheme.

NUMERICAL MODEL

The AC voltage applied to the electrodes of the DBDA ionizes the air in the vicinity of the electrodes and generates an electric field above the encapsulated electrode of a specific distribution depending on the form of the applied voltage The accelerated ionized air from the anode to the cathode in the presence of the generated electric field produces an electrohydrodynamic (EHD) force. This induced force acts as a body force vector that directly affects the flow field of the mainstream in that domain. Therefore, when applying Navier-Stokes equation to the main flow, this force must be considered in the equations as a source (body force) term. According to Suzen et al. [15] if all magnetic forces are neglected, the produced EHD force vector $\overrightarrow{F_b}$ can be expressed as follows:

$$\overrightarrow{F_b} = \rho_c \vec{E} \tag{1}$$

where: ρ_c is the net charge density and $\vec{E}$ is the electric field. As mentioned by Suzen et al. [15] the electric filed $\vec{E}$ can be evaluated from Maxwell's equations by assuming no time variation in the magnetic field as follows:

$$\vec{E} = -\nabla\Phi \tag{2}$$

where Φ is the total electric potential which equals the sum of the potential due to external electric field, ϕ, and the potential due to the net charge density of the plasma,φ ; i.e $\Phi = \phi + \varphi$.

As indicated by Bouchmal [10], the electric induction, $\vec{D}$ equals the electric field $\vec{E}$ times the permittivity ε of the medium, .i.e. $\vec{D} = \varepsilon\vec{E}$. The permittivity $\varepsilon = \varepsilon_r \varepsilon_o$, where; ε_r is the relative permittivity of the medium and ε_o is the permittivity of the free space. He indicated that according to Gauss law as given in Bouchmal [10]: $\nabla.\vec{D} = \rho_c$.
By substituting for $\vec{D}$ and $\vec{E}$ from Eq.(2) the following relation is obtained:

$$\nabla \cdot (\varepsilon \nabla\Phi) = -\rho_c \tag{3}$$

Based on the assumptions and method described in detail by Suzen et al. [15] Eq.(3) can be manipulated to be expressed in two independent equations , one for potential due to the external electric field (applied voltage on the electrodes),

$$\nabla \cdot (\varepsilon_r \nabla\phi) = 0 \tag{4}$$

and the second for the potential due to the charged particles in the plasma which can be rewritten in terms of the net charge density as given in Suzen et al. [15] as follows:

$$\nabla \cdot (\varepsilon_r \nabla \rho_c) = \rho_c / \lambda_d^2 \tag{5}$$

where λ_d is the Debye length.

Equations (4) and (5) are solved using Fluent User Defined Scalar (UDS) to get the field of both the electric potential ϕ and the net charge density ρ_c. The boundary conditions used for solving Eqns. (4) and (5) are shown in Fig. 2. Once ϕ and ρ_c are calculated a User Defined Function (UDF) is used to calculate the body force vector to be incorporated in the momentum equations from:

$$\overrightarrow{F_b} = \rho_c(-\nabla\phi) \tag{6}$$

The boundary condition of net charge density over the encapsulated electrode and the applied voltage imposed at the exposed electrode can be described respectively as:

$$\rho_c(t) = \rho_{c,max}\, f(t) \tag{7}$$

$$\phi(t) = \phi_{max}\, f(t) \tag{8}$$

where $\rho_{c,max}$, and ϕ_{max} are the maximum net charge density and maximum external potential allowed in the domain, respectively. The values of $\rho_{c,max}$ and λ_d are determined experimentally as described by Suzen et al. [15]. The function $f(t)$is the wave form function of the external applied voltage. For steady case, $f(t)$ can be set as a square wave. Since Eqns. (4) and (5) do not contain any time derivative term, they can be set in non-dimensional forms as shown in Fig. 2 . In these dimensionless forms, both the net charge density and electric potential fields are normalized as follows:

$$\rho^*_c = \frac{\rho_c}{\rho_{c,max}\, f(t)} \tag{9}$$

$$\phi^* = \frac{\phi}{\phi_{max}\, f(t)} \tag{10}$$

The dimensionless forms of Eqns. (4) and (5) lead to the use a unity for both the normalized charge density over the encapsulated electrode, ρ^*_c , and the normalized applied voltage imposed at the exposed electrode, ϕ^* as shown in Fig. 2. Accordingly, it will be possible to calculate the net charge density and the electric potential fields at any given time by multiplying the obtained distributions by the values $\rho_c(t)$, and $\phi(t)$, respectively. Consequently the DBDA body force vector can be estimated. The non-dimensional boundary conditions used in the UDF are shown in Fig. 2 for the non-dimensional parameters given by Eqs. (9) and (10).

The estimated DBDA body force vector is implemented into governing momentum equation as a source term. The DBDA simulation is carried out by solving Navier-Stokes equations for three-dimensional incompressible flow, steady state as:

$$\nabla \cdot (\rho U) = 0 \tag{11}$$

$$(\mathrm{U}\cdot\nabla)\rho\mathrm{U} = -\nabla p + F + \frac{\partial}{\partial x_j}(\tau_{ij} - \rho\overline{u_\iota u_j}) \tag{12}$$

$$\rho(\mathrm{U}\cdot\nabla\epsilon) - \nabla\cdot(K_H\nabla T) + p\nabla\cdot\mathrm{U} = 0 \tag{13}$$

where U is the average velocity component, ρ is the density of working fluid, p is the average pressure, F is the external applied force, τ is the molecular stress tensor, u is the local velocity component , ϵ is the thermodynamic internal energy, $\mathrm{K_H}$ is the heat conduction coefficient, and T is the average temperature.

GEOMETRY AND BOUNDARY CONDITIONS

The geometry of the turbine vane considered in the present study is shown in Fig. 3(a). The film cooling effectiveness is studied on the pressure side of this turbine vane. The two-dimensional aspects of the vane are listed in Table 1. The domain consists of a turbine vane along with the cooling setup which includes the plenum and the injection channel. The plenum dimensions as function of the injection hole diameter D are 6.5 D×13.25 D×4.5 D , the injection channel has a cylindrical hole of diameter D = 0.8 mm and is located at of 28 % of the axial chord with injection angle α = 22°. The channel has a lateral spacing of 4.5 D and a length-to-diameter ratio of 8.5 D. The inlet temperature of the main flow stream and the injected temperature of the coolant are 300 K and 150 K, respectively which satisfy the density ratio DR = 2 as specified by the experimental results of Ito, et al. [16]. The inlet velocity boundary condition is 14.1 m/s and the injected coolant velocity is calculated according to the required blowing ratio (BR).

The pressure outlet boundary condition is set at the exit face in the computational domain. The vane, plenum, and injection channel walls are considered no-slip boundaries. Also, a periodic boundary condition is set for the rest of the computational domain faces where only one repeated injection hole on the pressure vane side is considered. The height of the repeated domain region is z/D = 2.25 D.

Two plasma actuators are installed at the pressure side of the turbine vane surface downstream the film cooling hole. The dimensions of the actuator are shown in Fig. 4(a). The thickness of the exposed electrode is too small, so the exposed electrode can be assumed as a patch on the surface. Kapton and copper are adopted for the dielectric and electrode materials, respectively. The relative permittivity of air and Kapton are 1.0 and 2.7, respectively. The encapsulated electrode thickness is 0.102 mm and it is buried at a depth of 0.127 mm far from the vane surface. The width of exposed and encapsulated electrodes is 0.1 mm and 1.1 mm, respectively. The two plasma actuators are placed symmetrically along the injected flow axis. There is no underlap or overlap distance between the two electrodes along the blade height direction as shown in Fig. 4(a). The plasma actuators are located at 0.5 D downstream the injection hole and spaced by a distance of 0.25D as shown in Fig. 4(b). In the present study, there are two varying parameters of plasma actuators have been considered. One is the geometrical parameter which represents the actuator's length and the second is an operating condition which represents the applied voltage. The summary of the actuator length and applied voltage values considered are listed for different studied cases in Table 2.

In the present paper, the centerline film cooling effectiveness is defined as:

$$\eta_c = \frac{T_m - T_{adw}}{T_m - T_i} \tag{14}$$

Where T_m is the mainstream temperature, T_i is the injected coolant temperature and T_{adw} is the vane surface adiabatic wall temperature which varies along both the x and z directions.

The average film cooling effectiveness along the span-wise direction over a length of 4.5D is given as presented by:

$$\eta_{avg} = \frac{1}{4.5}\sum_{i=0}^{n} \eta_{c\,i}[\tfrac{z}{D}] \left|\{\left(\tfrac{\Delta z}{D}\right)\}_i\right| \tag{15}$$

The spatially-averaged film-cooling effectiveness is averaged over an area vane surface extends 4.5D span-wise and 48.16D stream- and is given by:

$$\eta_s = \frac{1}{4.5\times 48.16}\sum_{j=0}^{k}\sum_{i=0}^{n} \eta_{c\,i,j}[\tfrac{X}{D}, \tfrac{z}{D}] \left|\{\left(\tfrac{\Delta X}{D}\right)_j \times \left(\tfrac{\Delta z}{D}\right)_i\right| \tag{16}$$

The vorticity of the flow in the stream-wise direction is defined as:

$$\omega^* = \omega_x \frac{D}{u_m} \tag{17}$$

GRID INFORMATION AND NUMERICAL METHOD

A three dimensional domain around a turbine vane in a linear cascade was generated using GAMBIT 2.4 to study the film cooling effectiveness. The detailed mesh is shown in Figs. 3(b,c,d). Unstructured grids are used for the film cooling hole and the passage between the plenum and vane surface while structured grids are used for the rest of the domain. Five mesh sizes (0.41 M - 0.73 M - 1.22 M - 2.05 M - 3.59 M) have been individually investigated for mesh independency test. For each case, the film cooling effectiveness was calculated. The results of the calculated average film cooling effectiveness and the spatially-averaged film cooling effectiveness over the vane surface are shown in Figs. 5(a) and 5(b) , respectively. Fig. 5 shows that the sensitivity of both the predicted film cooling effectiveness decreases as the number of grid cells increases up to 2.05M. More grid cells than 2.05M do not significantly affect the solution. So, in the present study, the adopted number of cells is 2.05 M for reasonably good results and computational time.

For considering the viscous sublayer, special attention has been devoted to the cells' height near the walls. The height of the first cell is adopted to guarantee that, the wall distance y+ is less than unity as shown in Fig. 6.

The realizable k-ε model has been used in the present study because it has the ability to model successfully the aspect of the film cooling studies as reported by Zhang and Hassan [17]. ANSYS Fluent 16 has been used as a solver for the present

model. The solution criteria for the model consist of two steps. Firstly, the plasma actuator is being off while the film cooling model is solved for certain blowing ratios until a steady flow solution is acquired. Secondly, the plasma actuator with specified geometrical configuration is turned on until the obtained steady flow solution is converged. SIMPLE algorithm used as the solver for the pressure-velocity coupling. The second-order upwind scheme is used for the spatial discretization of the convective and normal diffusion terms while the cross-diffusion terms and the second order derivatives are discretized using central difference scheme. For each calculated parameter, the convergence criterion for the residuals is less than 1×10^{-6}.

VALIDATION OF THE MODEL

In order to validate the accuracy of the present numerical model solutions, the Mach number distribution calculated for case-0, base-line case, Table 2, is compared with the experimental results of Hassan and Hassan [18] . Figure 7(a) shows the distribution of Mach number over both the pressure side and suction side of the vane. It can be seen from this figure that the present computed results of the variation of Mach number with x/Cx for both vane sides are in very good agreement with the experimental results of Hassan and Hassan [18]. Also, Fig.7 (b) compares the present model results of the centerline effectiveness with the corresponding results of Sinha et al. [4], Ito et al. [16] and Walters and Leylek [19]. The figure indicates that the present results show good agreement with Sinha et al. [4] results for a flat plate model. On the other hand, minor discrepancies are observed between the present study results and those of Walters and Leylek [19] and Ito et al. [16] as shown in Fig. 7(b). Such discrepancies may be attributed to the difference in the vane geometry used in those studies compare with that used considered in the present study.

RESULTS AND DISCUSSION

In order to investigate the influence of applied voltage and actuator length on film cooling performance 25 cases have been considered in the present study as listed in Table 2. The effect of varying the voltage and actuator length on the vorticity contours, velocity and temperature distributions, effectiveness contours and on the centerline, span-wise average, and spatially averaged effectivenesses are presented and discussed below.

Dielectric Barrier Discharge Actuator (DBDA) Flow Control Mechanism for Cooling Improvement

In this section, a comparison between the performance of case-0, base line case, and case-9 for an actuator length = 5D, and applied voltage = 40 kV, at BR= 1.0 has been conducted to illustrate the effect of plasma actuation mechanism in improving film cooling effectiveness. As indicated above and in various previous works as Goldstein [1], Bunker [2], Li et al. [3], Sinha et al. [4]. The interaction between the cooling jet and the main stream without a DBDA generates a couple of CRVPs. The locations of the vortices accompanying the injection of the secondary (coolant) jet in the downstream direction along the vane surface at BR = 1.0 for three different cases determined and compared as presented and discussed below. These cases are; coolant injection without plasma actuation, plasma actuation without coolant injection

and coolant injection with plasma actuation. The strength and direction of rotation of the generated vortices (if any) that accompanying each case are shown in Fig. 8. From this figure, it is clear that in the case of coolant injection only, the generated CRVP are in the direction that causes mainstream entrainment beneath the secondary (coolant) jet. This in turn enhances the coolant jet detachment off the surface and result in reducing its cooling effectiveness. On the other hand, when the plasma is actuated on the surface without coolant injection, the generated vortices close to the surface are in the direction that helps lateral spreading of the secondary stream. From Fig. 8, it can be noticed that there are other two vortices located at about 0.2 D distance above the vane surface. Even if the mainstream is entrained inside the secondary jet as a result of the existence of those vortices, their impact is expected to be much lower than the CRVPs accompany the injection from the circular hole scheme without plasma because they will not cause jet lift off. When the plasma is actuated with secondary jet injection, the resulting vorticity distribution is the summation of the two previous cases as shown from Fig. 8.

Figure 9 presents the distribution of the z-velocity component perpendicular to the vane surface at z/D = 0.5 and at different axial locations for the above-mentioned cases (case-0, case-9 and plasma only). The figure indicates that there are significant changes in the velocity distribution observed for the case of coolant injection with no plasma actuation (case-0) compared with that for the case when plasma is actuated (case-9). For the case when no plasma is actuated, the z-velocity component is oriented towards the hole centerline which refers to a mainstream entrainment beneath the coolant jet. Contrarily, when plasma is applied without film cooling the z-velocity distribution is strongly oriented away from the hole centerline. It is clear from Fig 9 that the distribution for the case of plasma actuation with coolant injection is close to that for the case of plasma only, and consequently mitigates the effect that result from the interaction between the cooling jet and the main stream. This gives an indication of how plasma can be used to control jet lift off in film cooling applications.

Temperature Distribution

In order to demonstrate the influence of plasma actuator length and applied voltage on the coolant jet span-wise spreading, the temperature distribution on different vertical planes located at x/D = 2, 6 and 12 in the downstream of the injection holes are plotted, in Figs. 10 to 12, respectively. One of the important observations in Fig. 10 is that the change in the temperature distribution occurs mainly due to the change in applied voltage only, as is clear when rows and columns of the figure are compared. The plane at x/D = 2 is located at the end of the shortest actuator (L/D=1.5) and above the other investigated actuators for which L/D > 1.5. Based on this, it can be concluded that since the region downstream this plane, i.e. for x/D > 1.5, is affected by the actuator, the same performance will be obtained regardless of the actuator length after this location. The results presented in Figs. 11 and 12 support this conclusion. From Fig. 11, it is clear that the changes in the temperature distribution on the plane at x/D =6 are observable for the cases with actuator length less than 6D. For the cases where the length of the actuator is larger than 6D, the same temperature distribution is obtained which is an effect similar to that occurs in the case of x/D = 2. The distributions shown in Fig. 12 are those for a plane located at x/D = 12 close to the end of the longest actuator (L/D=12) investigated in the

present work. Thus, the effect of actuator length on the temperature distributions is clear and pronounced for all presented cases as shown in the figure.

Careful inspection of the temperature distributions described above indicates that the applied voltage value does not always have a positive impact all the time and might result in a negative effect on the performance. This is clear in the far downstream locations when a high voltage is applied in the case with large x/D as shown in Fig. 12. In such case, the newly generated vortices resulted in significant secondary jet spreading far from the hole centerline and away from the vane surface. This in turn is expected to have a negative impact on the cooling effectiveness as shown and discussed below.

Effect of Applied Voltage on the Film Cooling Effectiveness

Figure 13(a) and 13(b) is the film cooling effectiveness contours downstream the circular hole scheme without (case-0) and with plasma actuation (case-9), respectively. Significant enhancement in the case when the plasma is actuated is observable when compared with the case with no plasma. The enhancement is observable in both the downstream and span-wise directions, which is a highly preferred for any film cooling application. When the span-wise averaged effectiveness is compared for different actuator length, Fig. 14, the trend of effectiveness enhancement is not the same in all cases. For the case of actuator length = 1.5D, as the applied voltage is increased, the span-wise averaged effectiveness is enhanced all over the region of interest in the downstream direction. Also, it is clear that the effectiveness starts to increase as soon as the actuator starts on the vane surface and starts to decay once the actuator end is reached. When the actuator length is increased, the effect of the applied voltage far downstream starts to have a negative impact for all cases other than the case of L = 1.5D, as Fig. 14 shows. When such performance is averaged all over the region of interest in the form of spatially averaged effectiveness, Fig. 15(a), the trend of effectiveness performance with the change in actuator length and applied voltage is very clear. From Fig. 15(a), it is clear that for each actuator length there is an optimal voltage value that must be applied to achieve the maximum possible performance. In case of long actuator length, low value of applied voltage is needed compared to that recommended for short actuators to achieve such performance. The same information can be extracted from Fig. 15(b).

Effect of Blowing Ratio

The effect of lowing ratio is studied for the best case, case-9, where an optimum film cooling performance is obtained compared to all studied cases. Figure 16 shows that the existence of plasma actuation enhances the film cooling effectiveness at any blowing ratio, when compared with the case with no plasma. However; the degree of enhancement is not the same for all blowing ratios. The maximum enhancement is obtained at BR = 1.0 for which the momentum perpendicular to the vane surface is lower that the cases of BR = 1.5 and 2.0 and as a result the influence of the generated body force is more significant for the same applied voltage and actuator length.

CONCLOSION

The effect of plasma actuator length and applied voltage on the film cooling performance of a circular hole scheme was numerically investigated over a gas turbine vane pressure side. The investigation was carried out at unity blowing ratio for the majority of the study, and the effect of varying the blowing ratio was investigated for the case with the best cooling effectiveness only. Five applied voltages and five different actuator lengths have been considered in the investigation. The results show the formation of a vortex pair under the effect of plasma actuation opposite in direction to the CRVP accompanying the injection from a circular hole scheme without plasma. The presence of such anti-vortex pair led to improved lateral jet spreading in the span-wise direction and controlled jet lift-off. Consequently, the averaged film cooling effectiveness achieved was much higher when compared with the case of no plasma. Meanwhile, for each considered actuator length, the spatially averaged effectiveness was enhanced with the increase of the applied voltage to a certain limit where it reaches a maximum value, then the effectiveness decreases with the increase of the voltage. for each considered actuator length, the spatially averaged effectiveness was enhanced with the increase of the applied voltage to a certain limit where it reaches a maximum value, then the effectiveness decreases with the increase of the voltage.

8 – References

[1] R. J. Goldstein, "Film Cooling ", 7, pp. 321-379 (1971).
[2] R. S. Bunker, " A Review of Shaped Hole Turbine Film-Cooling Technology ", Journal of Heat Transfer, 127(4), p. 441 (2005).
[3] H. Li, W. Ghaly and I. Hassan, "The Formation of Counter-Rotating Vortex Pair and the Nature of Liftoff-Reattachment in Film-Cooling Flow", Fluids, 1(4): p. 39, (2016).
[4] A. K. Sinha, D. G. Bogard and M.E. Crawford, "Film-Cooling Effectiveness Downstream of a Single Row of Holes with Variable Density Ratio", Trans. ASME, 113, p.p. 442–449 (1991).
[5] A. M. M. Abdala and F. N. M. Elwekeel, "Pressure Distribution Effects due to Chevron Fences on Film Cooling Effectiveness and Flow Structures", Applied Thermal Engineering, 110: p. 616-629 (2017).
[6] G.-C. Li and W. Zhang,"Improving Film Cooling Performance by Using One-Inlet and Double-Outlet hole", Journal of Thermal Science, 19(5): p. 430-437 (2010).
[7] S. Park, E. Y. Jung, S. H. Kim, H.-S. Sohn and H. H. Cho, "Enhancement of Film Cooling Effectiveness Using Backward Injection Holes", International Journal of Thermal Sciences, 110: p. 314-324 (2016).
[8] S. Na and T. I. P. Shih, "Increasing Adiabatic Film-Cooling Effectiveness by Using an Upstream Ramp", Journal of Heat Transfer, 129(4): p. 464 (2007).
[9] W. Zhou and H. Hu, "Improvements of Film Cooling Effectiveness by Using Barchan Dune Shaped Ramps", International Journal of Heat and Mass Transfer, 103: p. 443-456 (2016).
[10] A. Bouchmal, “Modeling of Dielectric-Barrier Discharge Actuator,” Master of Science Thesis, Delft University of Technology, (2011).
[11] C.-C.Wang and S. Roy, "Electrodynamic Enhancement of Film Cooling of Turbine Blades", Journal of Applied Physics, 104(7): p. 073305 (2008).

[12] J.-L. Yu, W. Ding, L.-m. He, Y. Wang and Y. Zhu ,"Numerical Simulation of The Effect of Plasma Aerodynamic Actuation on Improving Film Hole Cooling Performance ", Heat and Mass Transfer, 49(6): p. 897-906 (2013).
[13] S.-J. Dai, Y. Xiao, L.-M. He, T. Jin, Q. Zhang, P.-h. Hou and Z.-C. Zhao, "Film-cooling of Cylindrical Hole with Downstream Surface Dielectric Barrier Discharge Actuators", International Journal of Heat and Mass Transfer, 90: p. 825-837 (2015).
[14] S.-J. Dai, Y. Xiao, L.-M. He, T. Jin, Q. Zhang, P.-h. Hou and Z.-C. Zhao, "Computational Study of Plasma Actuator on Film Cooling Performance for Different Shaped Holes ", AIP Advances, 5(6): p. 067104 (2015).
[15] Y. B. Suzen, P. G. Huang and D. E. Aships,"Numerical Simulations of Flow Separation Control in Low Pressure", 45th AIAA Aerospace Sciences Meeting and Exhibit., Reno, Nevada, 8 - 11 January (2007).
[16] S. Ito, R. J. Goldstein and E. R. G. Eckert, "Film Cooling of a Gas Turbine Blade", Journal of Engineering for Power, VOL 100 (1978).
[17] C. X.-Z. Zhang and I. Hassan, "An advanced Louver Cooling Scheme for Gas Turbines-Part 1 Effectiveness", ASME Summer Heat Transfer Conference, USA (2005).
[18] O. Hassan and I. Hassan, "Experimental Investigations of the Film Cooling Effectiveness of a Micro-Tangential-Jet Scheme on a Gas Turbine Vane", International Journal of Heat and Mass Transfer, 61: p. 158-171 (2013).
[19] D. K. Walters and J. H. Leylek. "Computational Study Of Film-cooling Effectiveness On A Low-speed Airfoil Cascade - PART I: Methodology and Validation", ASME Design Technical Conferences, Canada (2002).

Table 1. The test vane geometrical parameters.

Parameter	Dimension, mm
True Chord, C	60.1
Axial Chord , Cx	38.88
Pitch , p	53.8

Table 2. The test matrix of the cases considered in the present study.

Case Number	Length/D	Applied Voltage, kV
Case-0	*Base-line case*: a circular hole scheme *without DBDA*	
Case-1	1.5	10
Case-2		15
Case-3		25
Case-4		40
Case-5		60
Case-6	3	10
Case-7		15
Case-8		25
Case-9		40
Case-10		60
Case-11	5	10
Case-12		15
Case-13		25
Case-14		40
Case-15		60
Case-16	8	10
Case-17		15
Case-18		25
Case-19		40
Case-20		60
Case-21	12	10
Case-22		15
Case-23		25
Case-24		40
Case-25		60

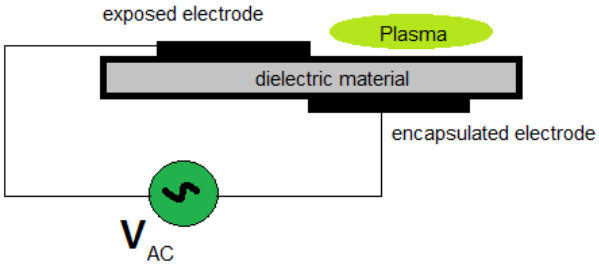

Fig.1: Dielectric Barrier Discharge Actuator components.

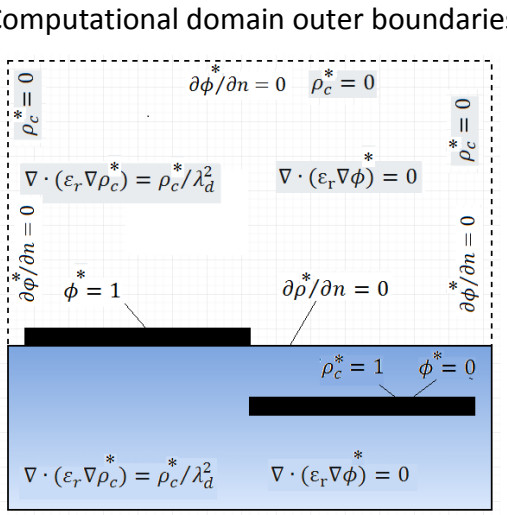

Fig. 2: The non-dimensional form and boundary conditions of Eqs. (4) and (5)

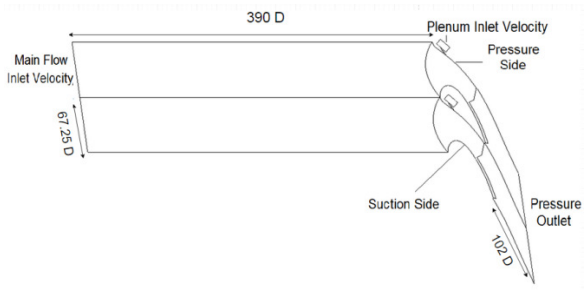

a) A two-dimensional geometrical schematic of the vane considered in the present model (doubled domain).

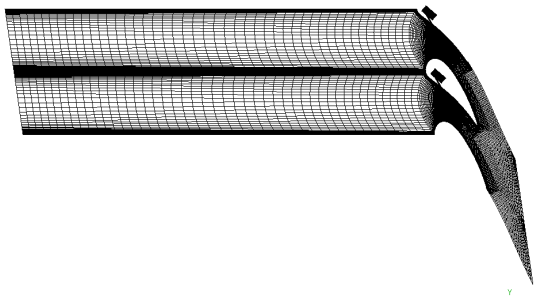

b) The domain mesh (doubled domain).

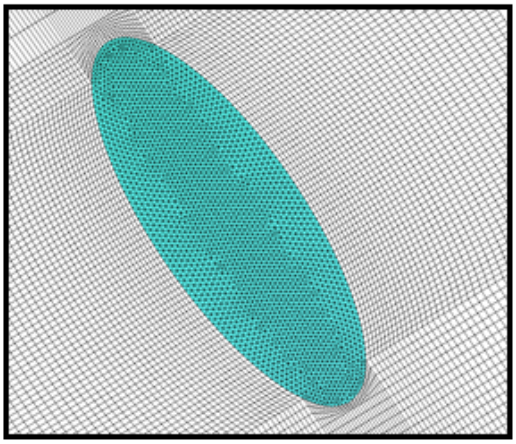

c) Hole unstructured grid.

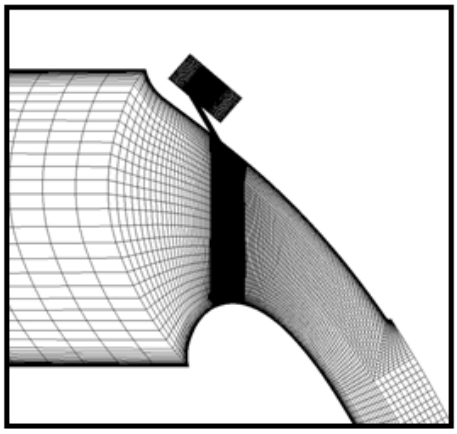

d) Enlarged grid near airfoil vane.

Fig. 3. A two-dimensional geometrical schematic of the vane considered in the present model and the grids used in the computation (doubled domain).

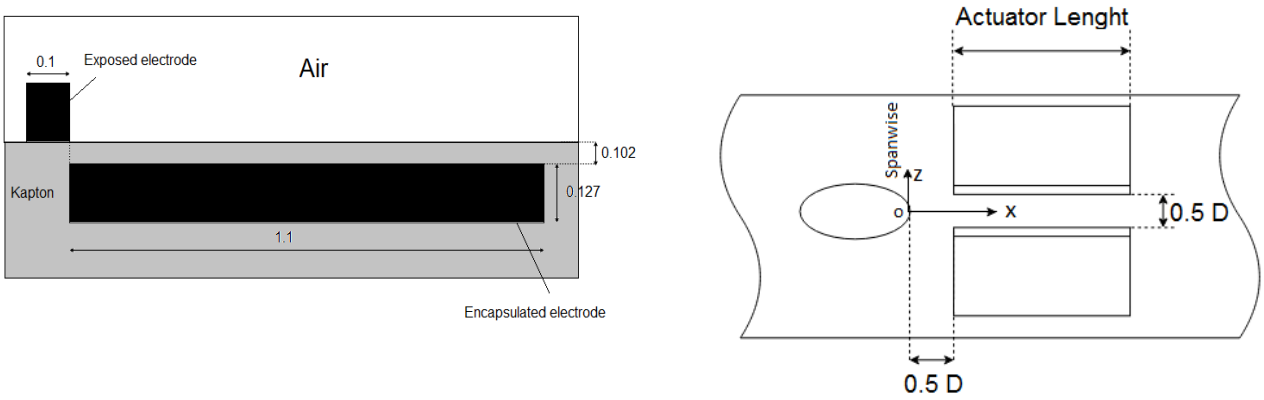

a) Dimension of DBDA in mm b) Location of DBDA

Fig. 4. Dimensions and location of the DBDA downstream the injection hole.

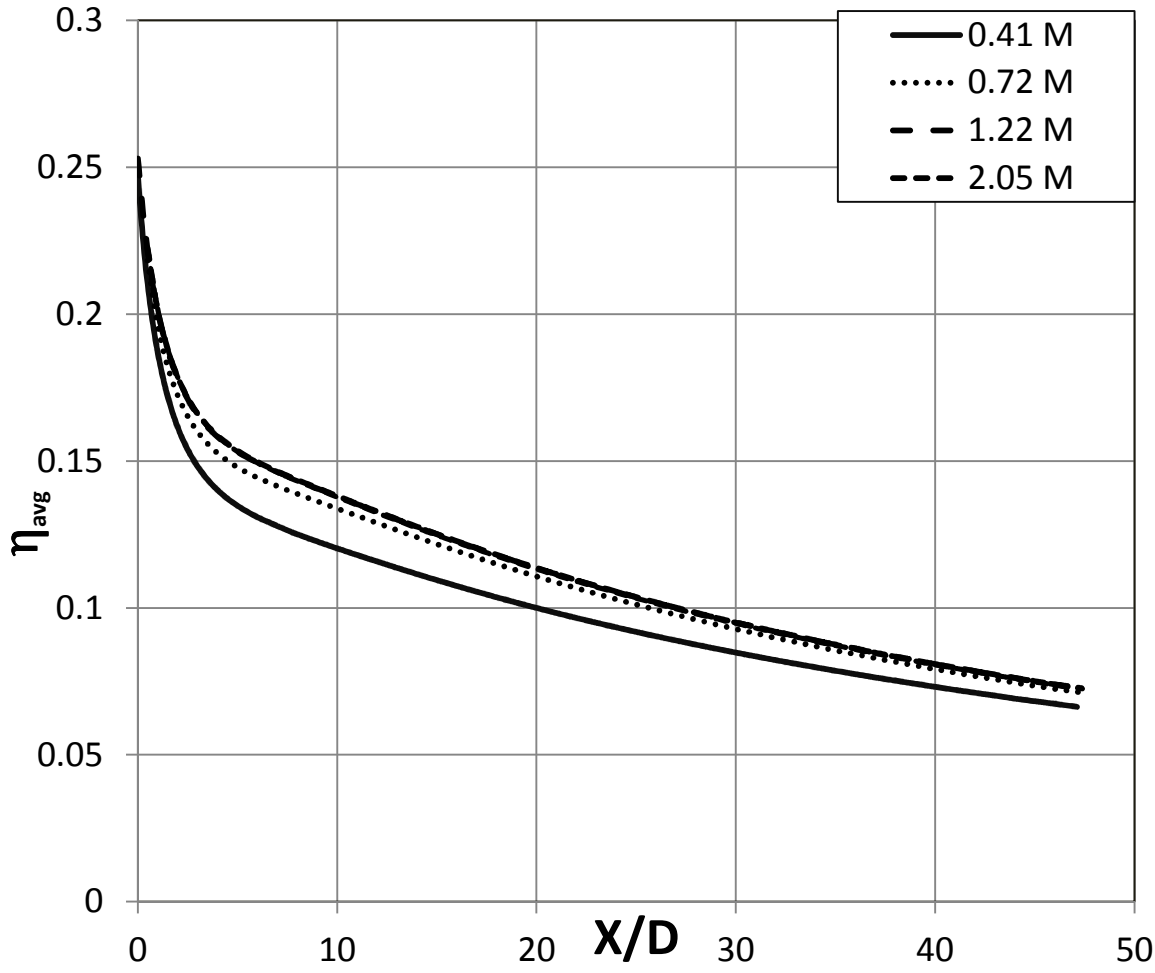

a) Grid sensitivity effect on average effectiveness η_{avg} (BR= 1).

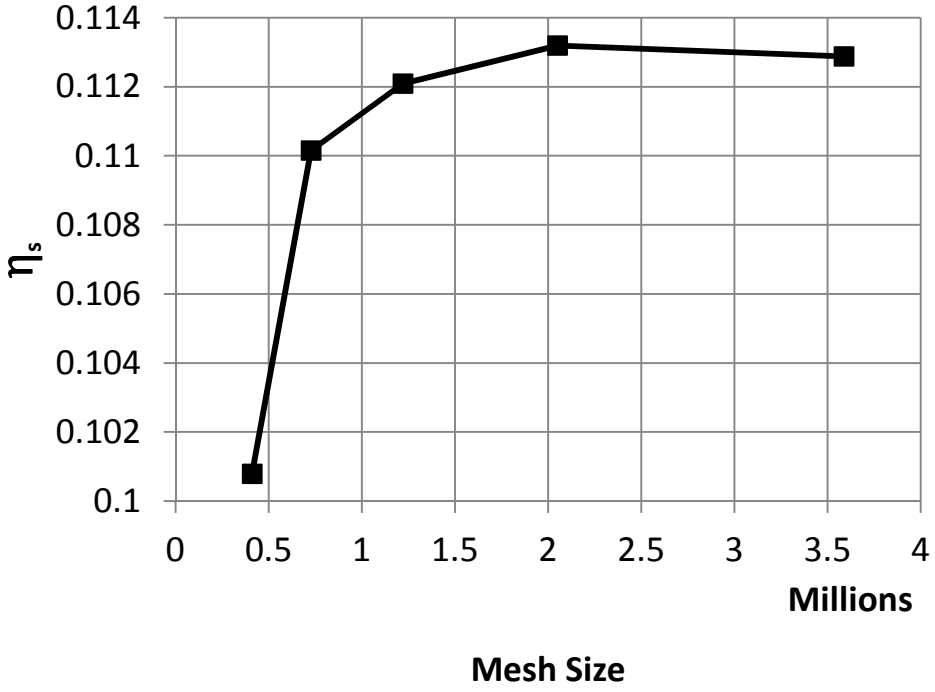

b) Grid sensitivity effect on spatially-averaged η_s (BR= 1).

Fig.5. Grid sensitivity test.

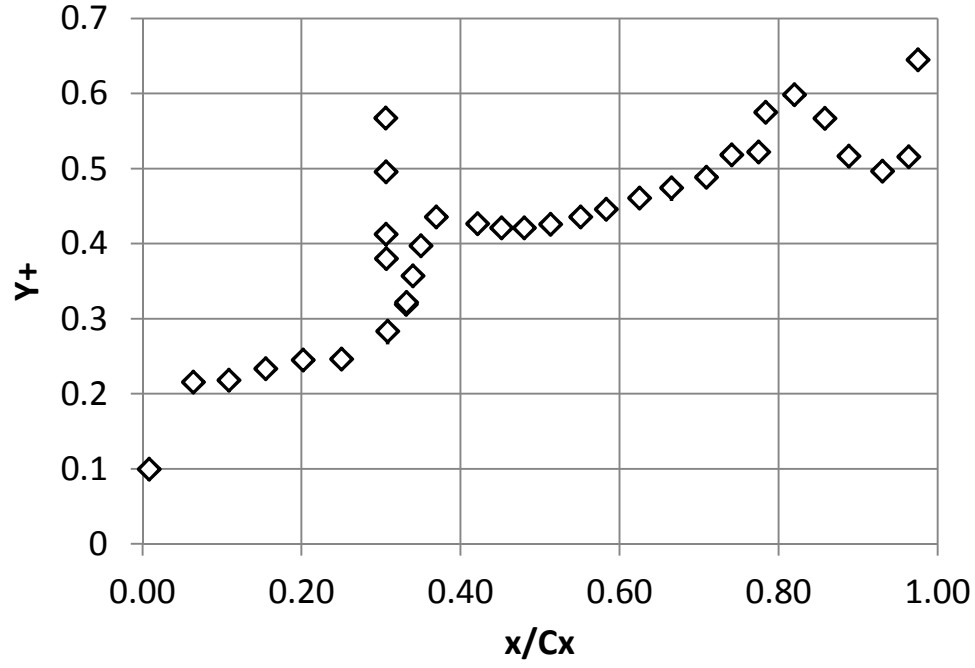

Fig. 6. Variation of the value of the wall distance y^+ over the vane surface.

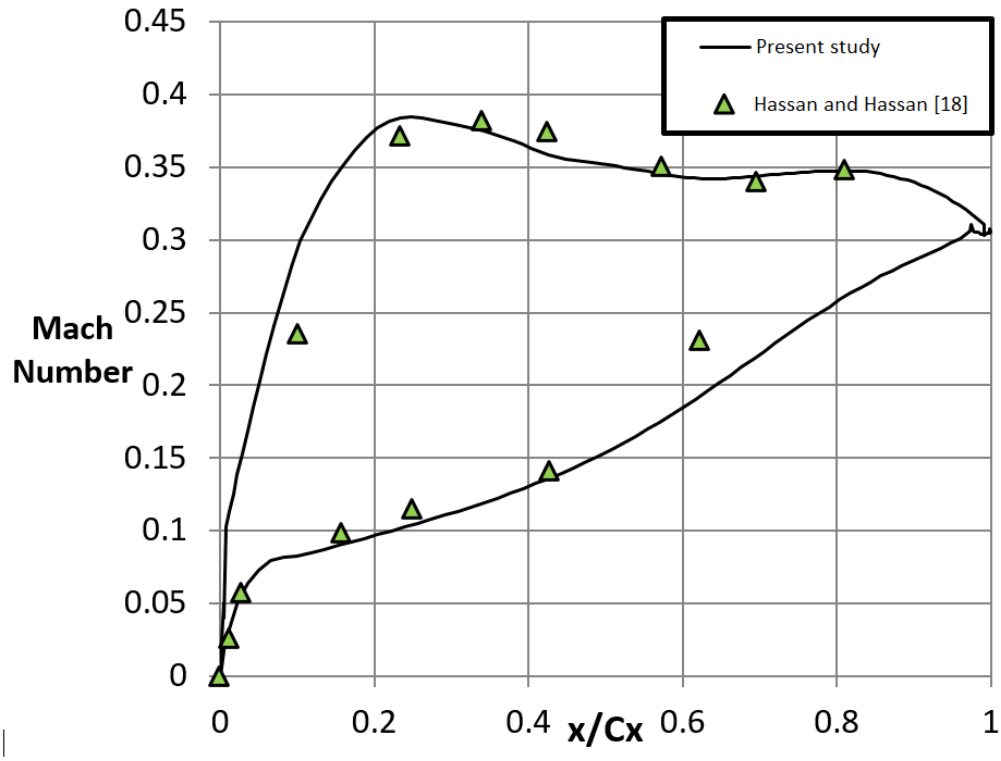

a) Comparison of Mach number distribution over the vane surface.

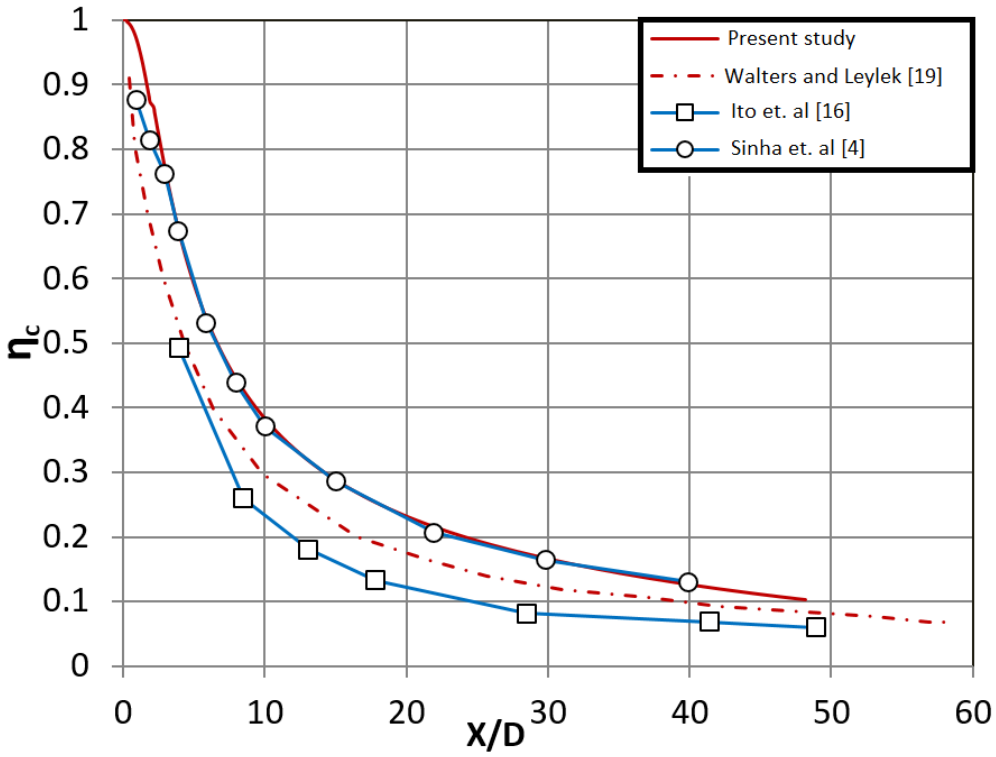

b) Comparison of centerline film cooling effectiveness (BR=0.5,DR=2)

Fig. 7. Validation of the present model results with the results of previous studies.

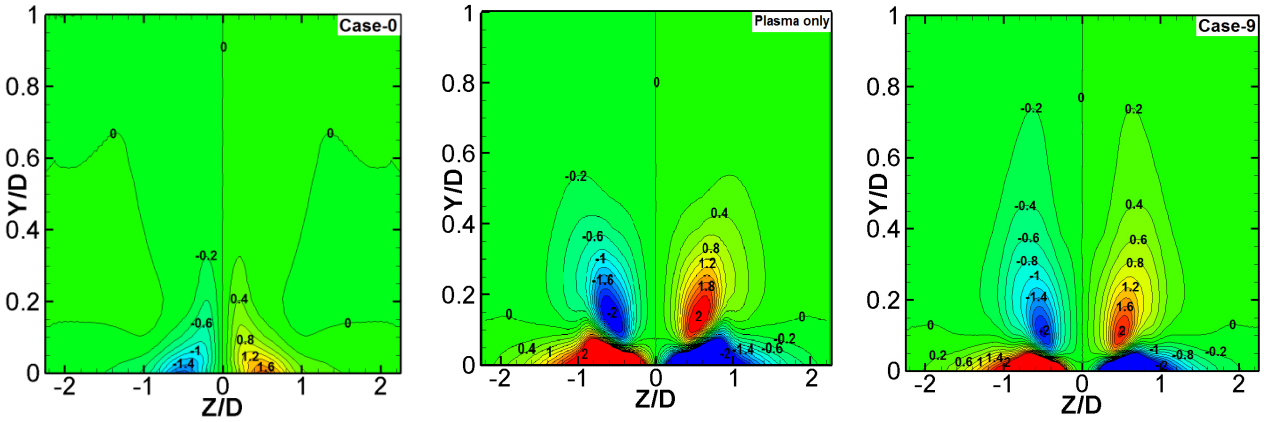

a) X/D = 2

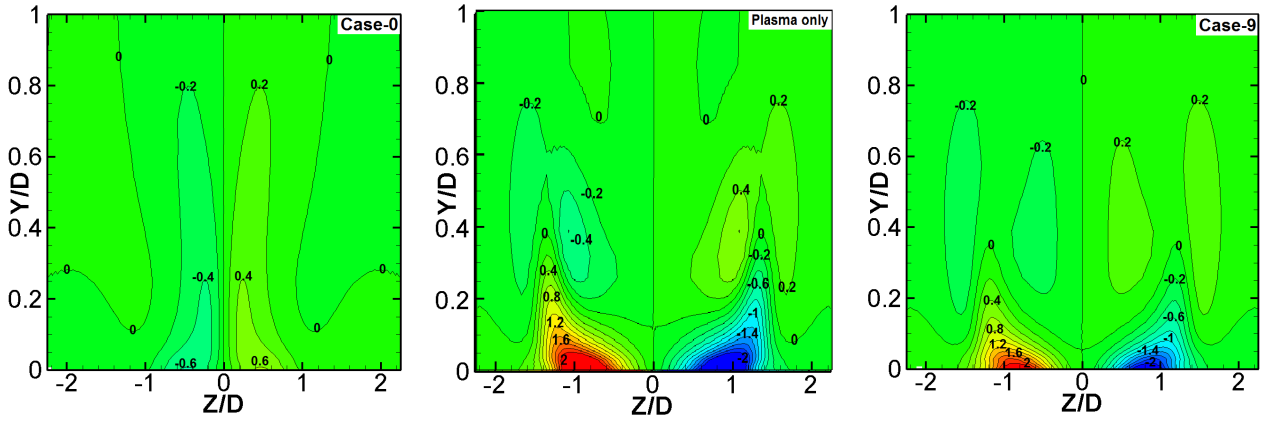

b) X/D =6

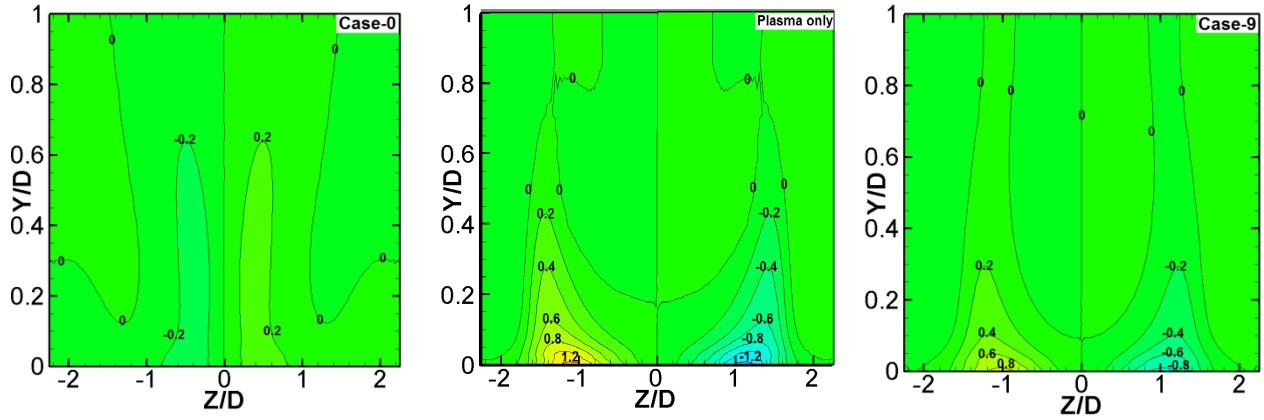

c) X/D =12

Fig. 8. The vorticity distribution for secondary (coolant) jet at BR = 1.

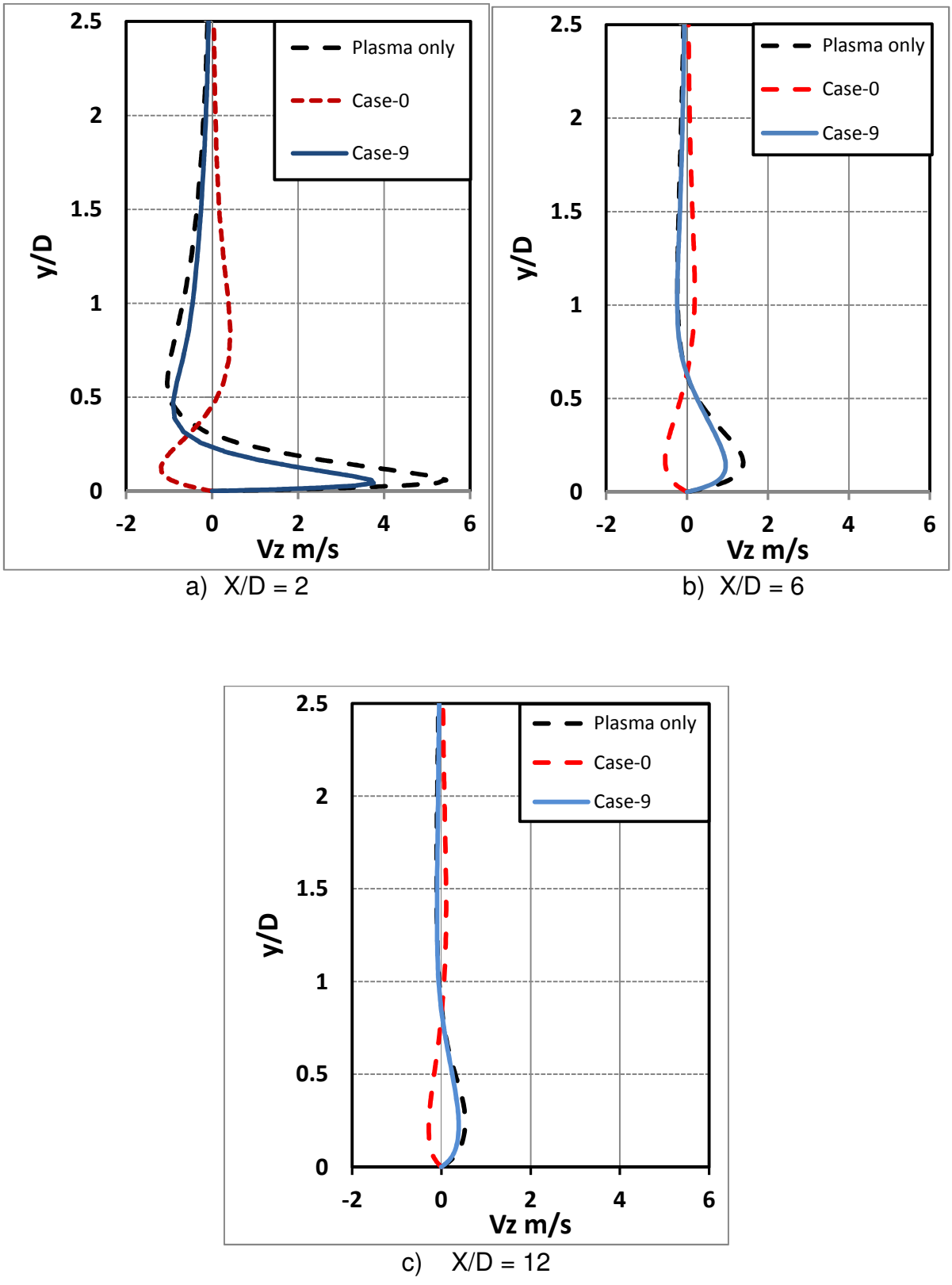

a) X/D = 2

b) X/D = 6

c) X/D = 12

Fig. 9. The distribution of the z-velocity component perpendicular to the vane surface at z/D = 0.5 for different axial locations.

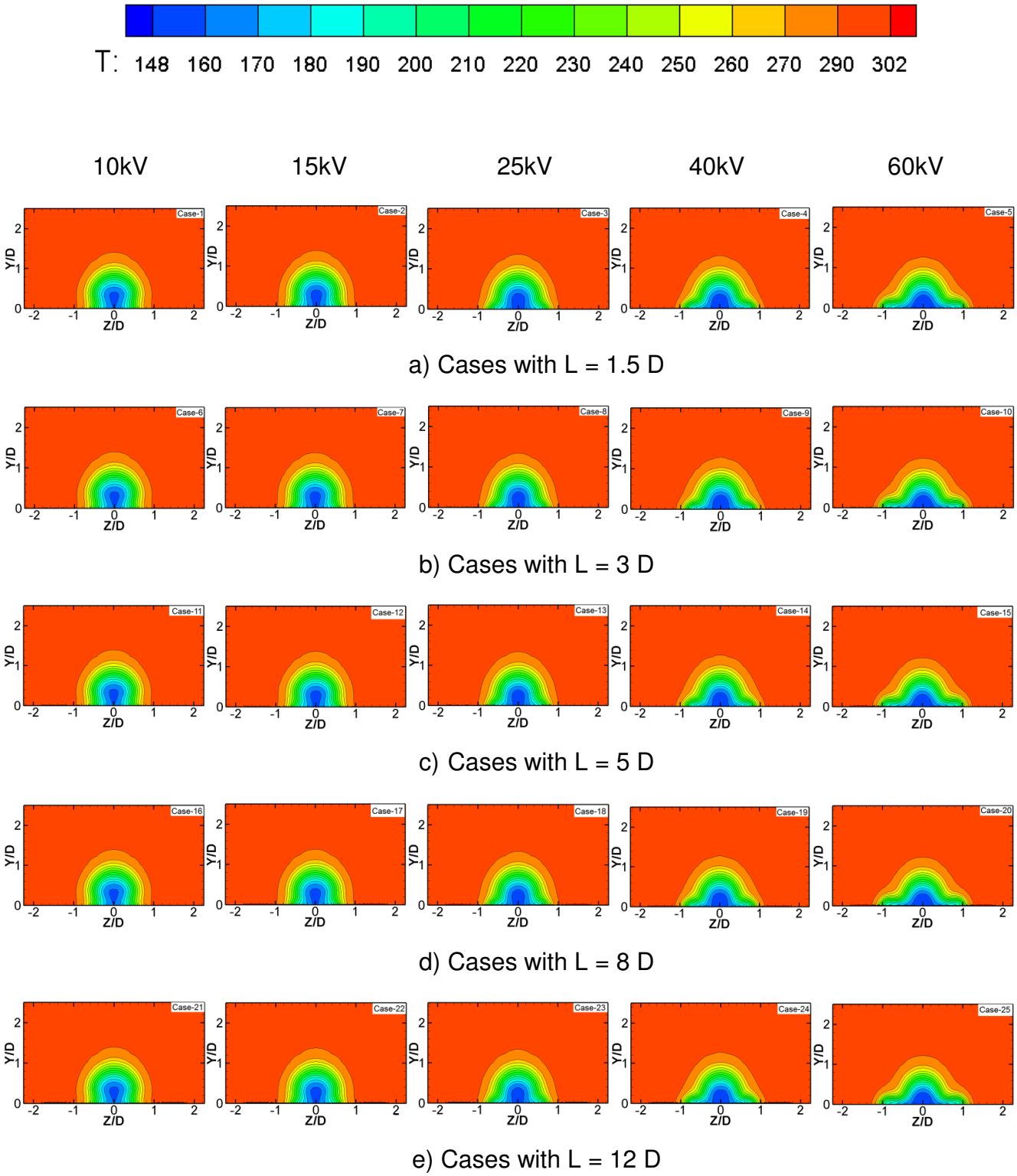

Fig. 10. Temperature distribution on the vertical plane at X/D=2.

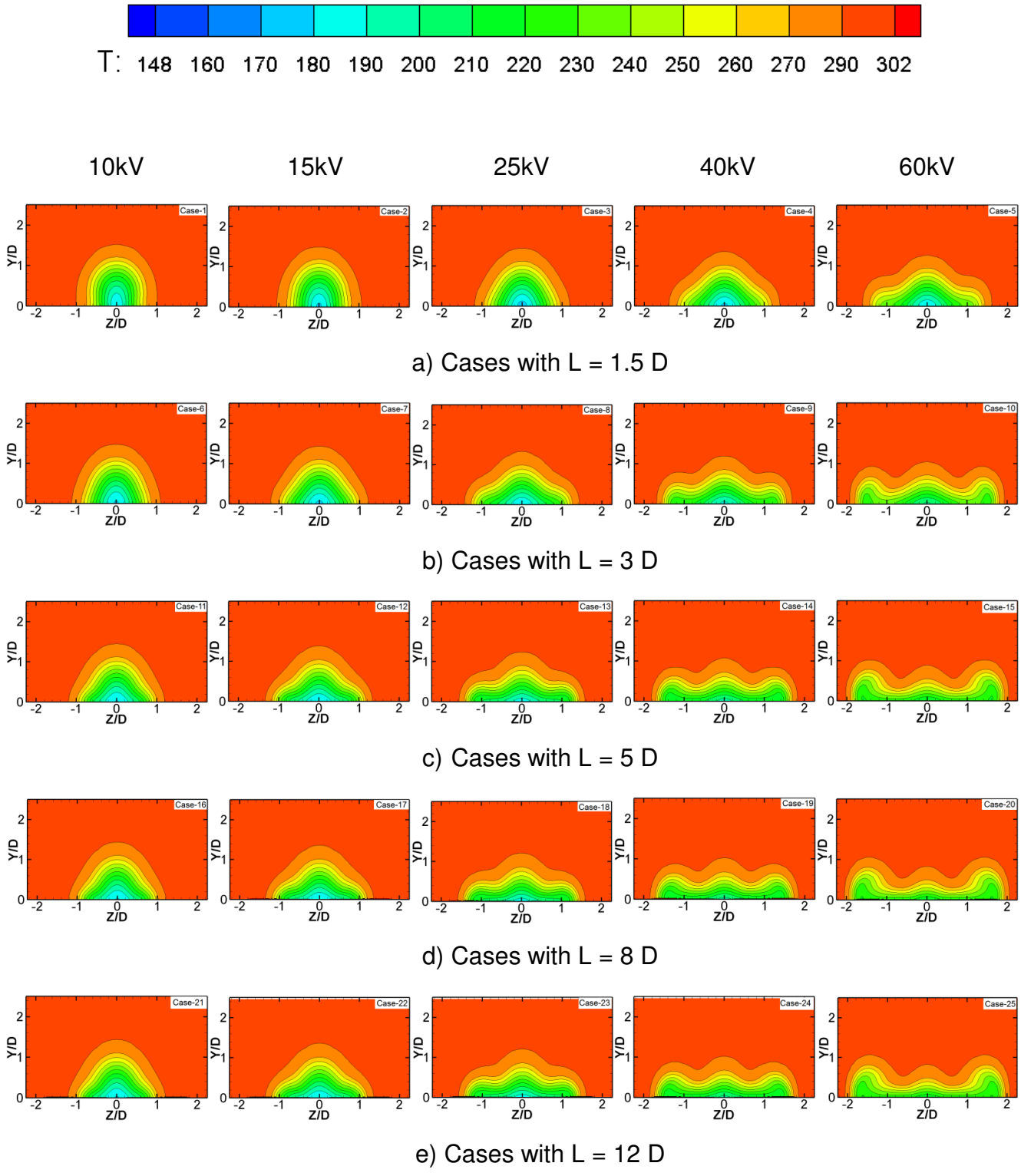

Fig. 11. Temperature distribution on the vertical plane at X/D=6.

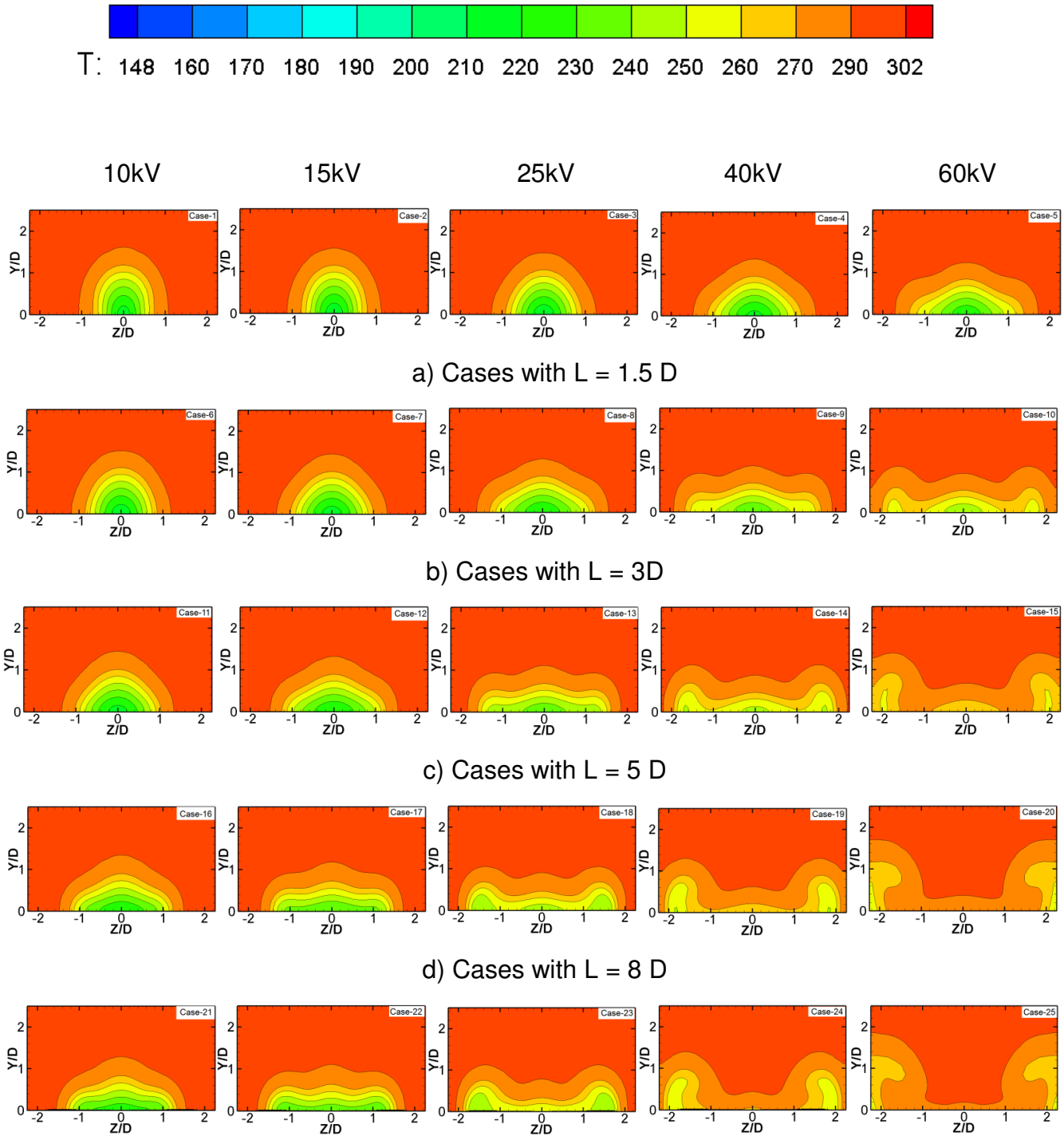

Fig. 12. Temperature distribution on the vertical plane at X/D=12.

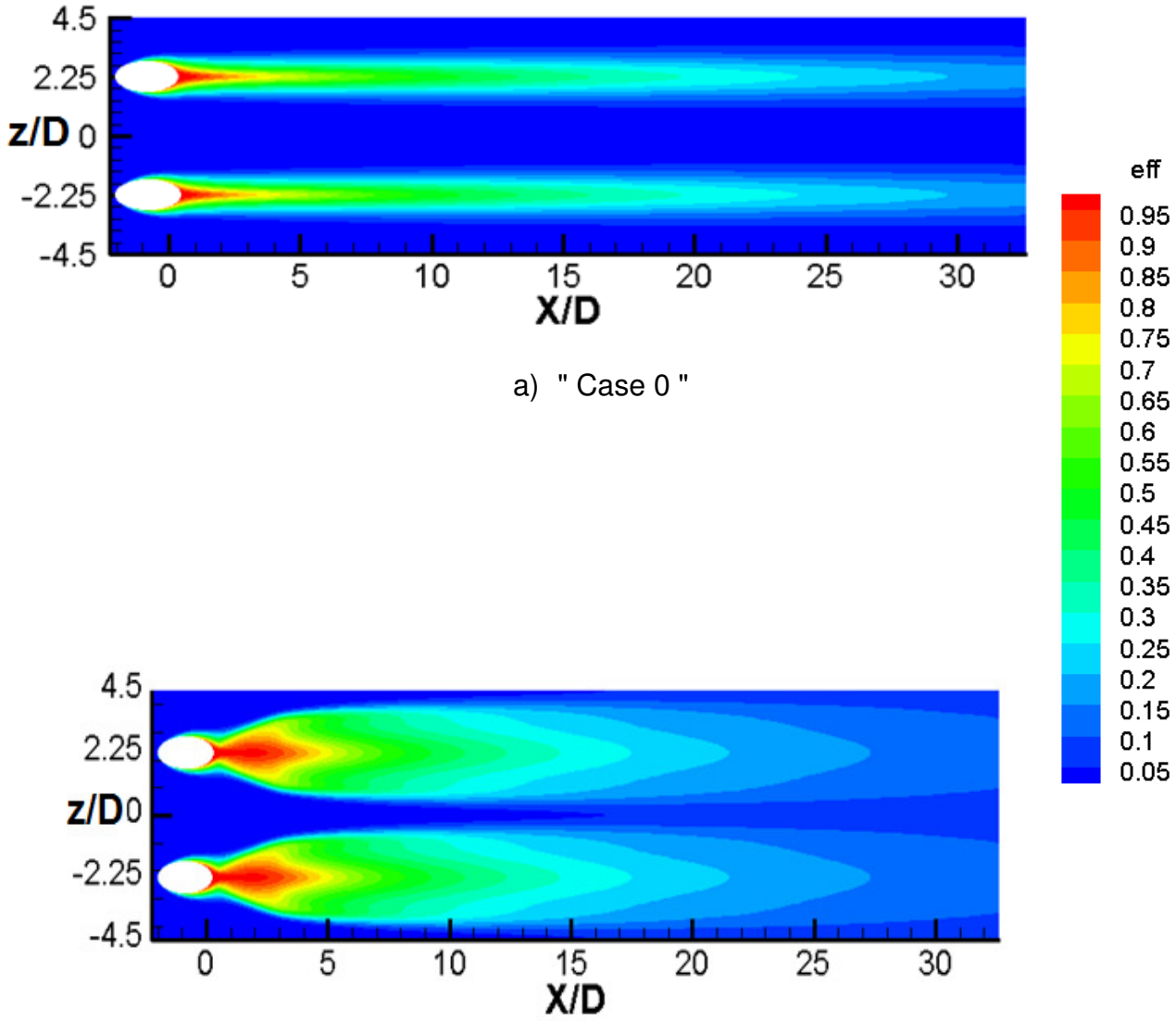

a) " Case 0 "

b) " Case 9 "

Fig. 13. Effectiveness contours over the vane surface (BR = 1.0).

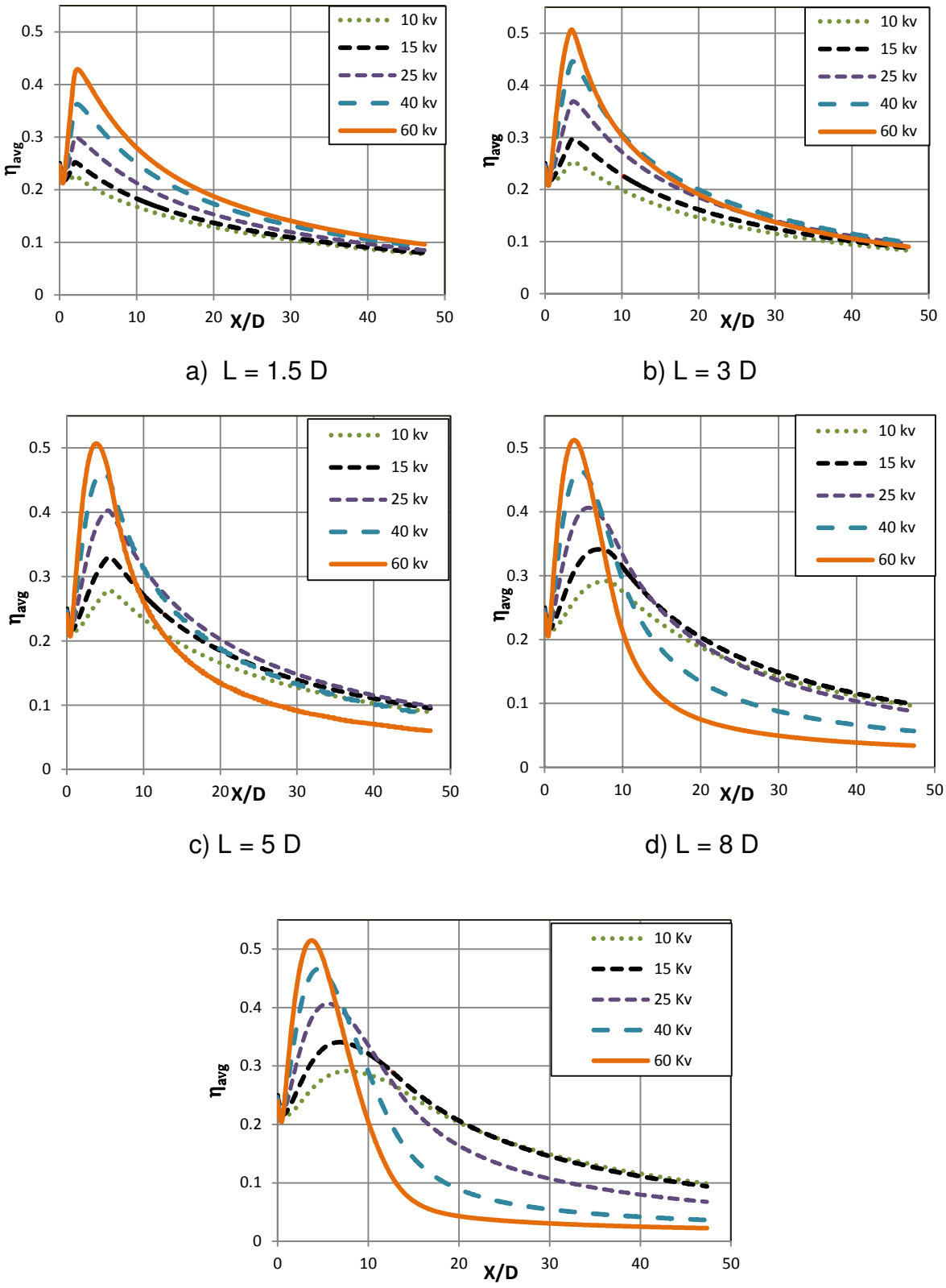

Fig. 14. Variation of span-wise averaged film cooling effectiveness in the downstream direction with the applied voltage for different actuator lengths.

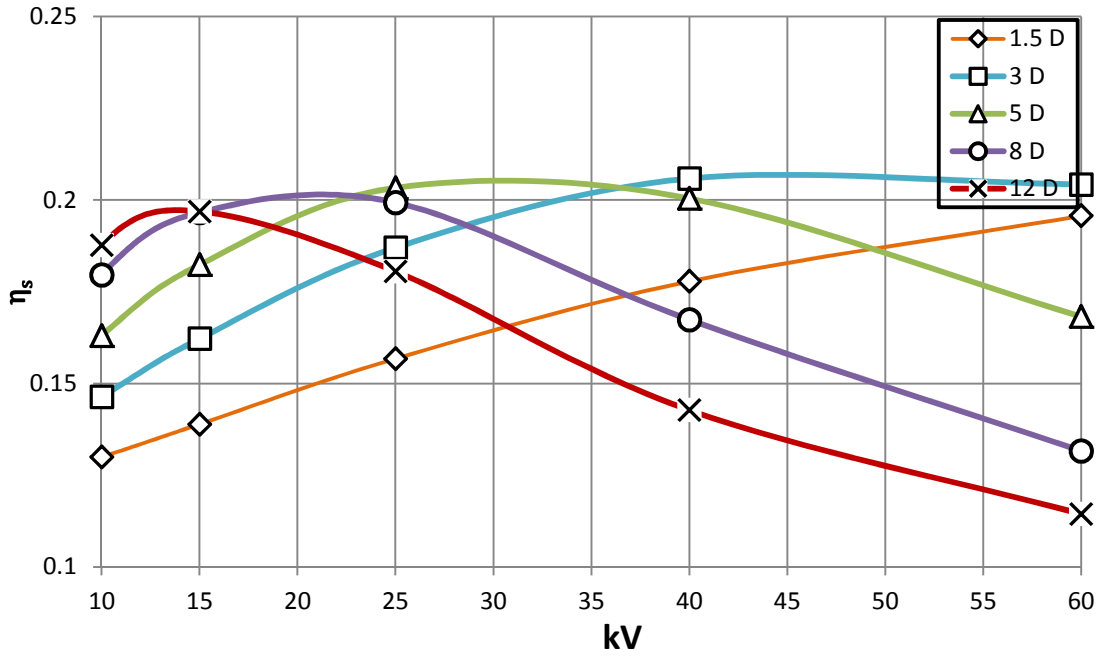

a) Variation of spatially-averaged film cooling effectiveness with the applied voltage for different actuator length.

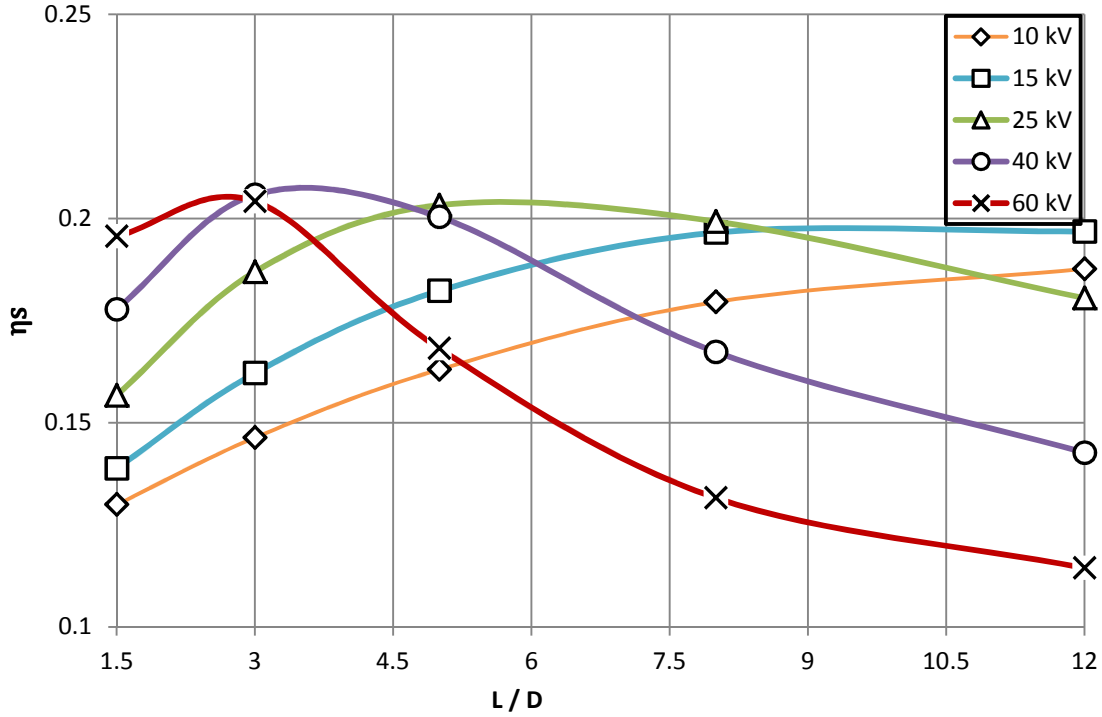

b) Variation of spatially-averaged film cooling effectiveness with the actuator length for different applied voltages.

Fig. 15. Spatially-averaged film cooling effectiveness variation with the applied voltage and actuator length.

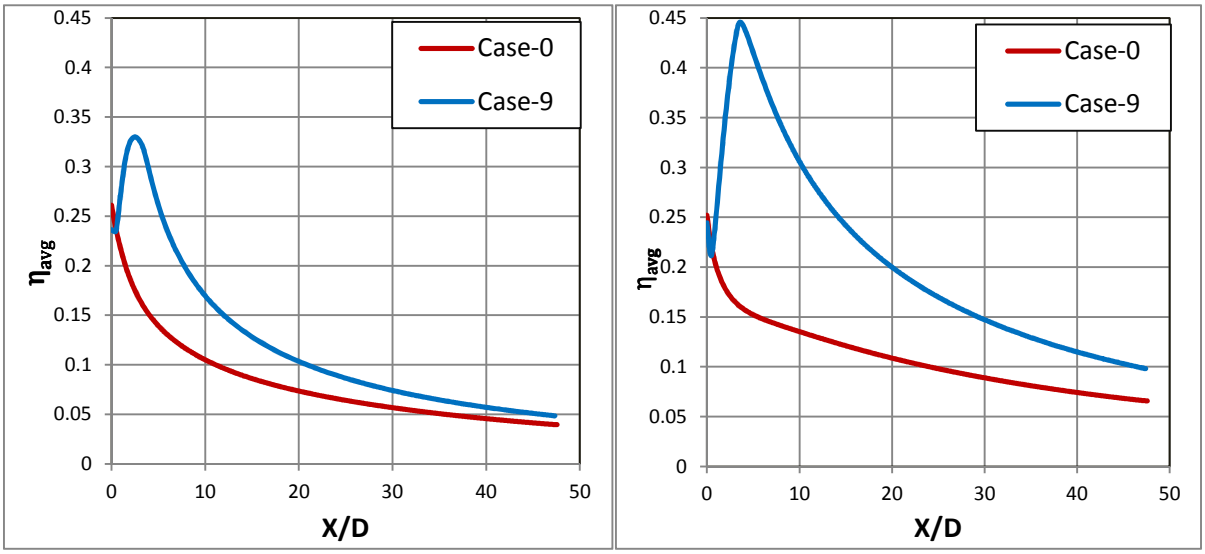

a) BR=0.5 b) BR=1

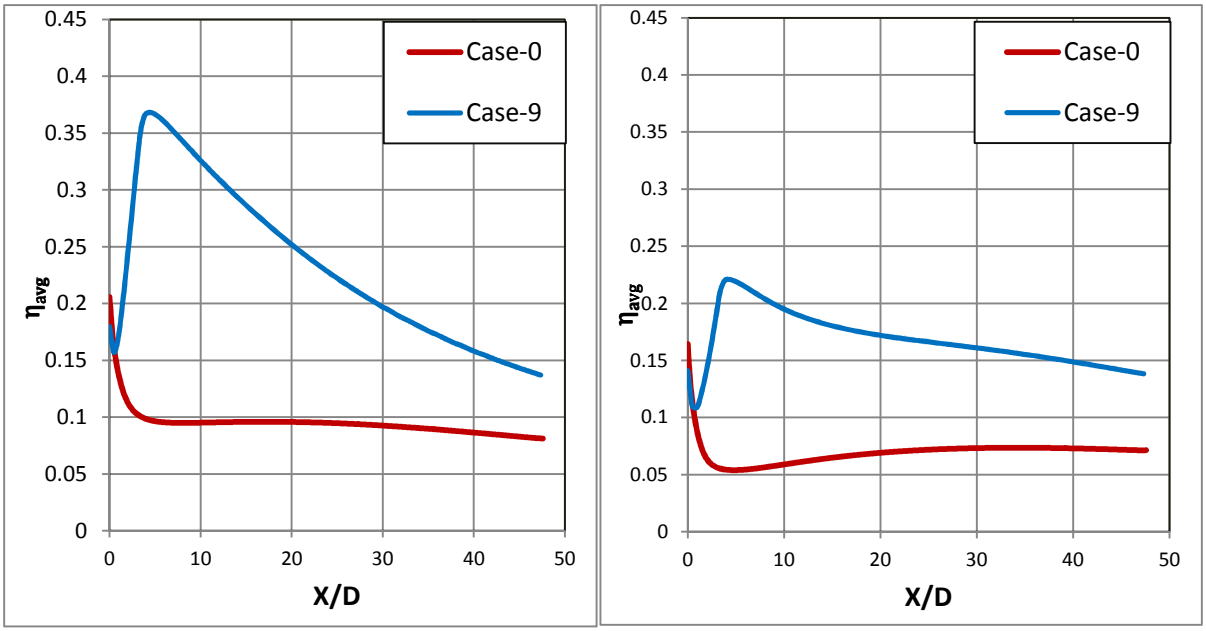

c) BR=1.5 d) BR=2

Fig. 16. Variation of the stream-wise average film cooling effectiveness in the down-stream direction for different blowing ratios, BR.